Structural Engineering and Mechanics, Vol. 36, No. 4 (2010) 463-479
DOI: http://dx.doi.org/10.12989/sem.2010.36.4.463

Dynamic reliability of structures: the example of multi-grid composite walls

Pei Liu* and Qian-Feng Yao[a]

School of Civil Engineering, Beijing Jiaotong University, Beijing, 100044, China

(Received March 1, 2010, Accepted July 13, 2010)

Abstract. Based on damage accumulation of multi-grid composite walls, a method of dynamic reliability estimations is proposed. The multi-grid composite wall is composed of edge frame beam, edge frame columns, grid beams, grid columns and filling blocks. The equations including stiffness, shear forces at filling blocks cracking and multi-grid composite walls yielding, ultimate displacement, and damage index are obtained through tests of 13 multi-grid composite wall specimens. Employing these equations in reliability calculations, procedures of dynamic reliability estimations based on damage accumulation of multi-grid composite walls subjected to random earthquake excitations are proposed. Finally the proposed method is applied to the typical composite wall specimen subjected to random earthquake excitations which can be specified by a finite number of input random variables. The dynamic reliability estimates, when filling blocks crack under earthquakes corresponding to 63% exceedance in 50 years and when the composite wall reach limit state under earthquakes corresponding to 2-3% exceedance in 50 years, are obtained using the proposed method by taking damage indexes as thresholds. The results from the proposed method which show good agreement with those from Monte-Carlo simulations demonstrate the proposed method is effective.

Keywords: dynamic reliability; damage accumulation; multi-grid composite walls; damage index; random earthquake excitation.

1. Introduction

Multi-grid composite wall structure created by the second author plotted in Fig. 1 is a new structural system, in which multi-grid composite walls are the primary lateral force-resisting components. The multi-grid composite wall is composed of autoclaved aerated concrete filling blocks, RC edge frame beam, edge frame columns (or connection column), grid beams, and grid columns. There are three stages for multi-grid composite walls of shear failure mode to dissipate earthquake energy. At the first stage, attributed to the restriction of RC edge frame and grids, there are no or very few cracks in the filling blocks. The mechanical behavior of the multi-grid composite wall is similar to that of an elastic panel. At the second stage, attributed to the low strength of filling blocks, there are a lot of cracks in them. RC grids and cracked filling blocks form the main member to resist earthquakes. At the third stage, the composite wall deteriorates into a frame made

*Corresponding author, Ph.D., E-mail: liupei0130@126.com
[a]Professor

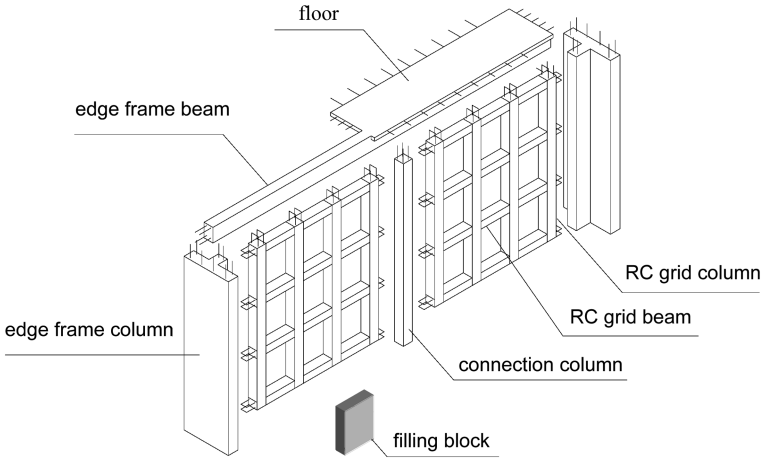

Fig. 1 Multi-grid composite wall structure

up of edge frame beam, edge frame columns and grid columns, and some plastic hinges appear on grid beams. At the end of the third stage, the composite wall reaches the limit state. And the multi-grid composite wall as the main force-resisting component of the structure fails, but it can bear all of the vertical loads and possess good capacity to resist collapse.

The current trend toward performance-based design requires the development of methodologies for accessing whether a given design satisfied engineering objectives (Chau and Albermani 2003, Xue and Chen 2003, Zhang and Foschi 2004, Chau 2007, Cheng *et al.* 2007, Augusti and Ciampoli 2008, McMillan and Brasington 2008). Several procedures for the structural reliability evaluation have been proposed (Dymiotis *et al.* 1999, 2001, Takada and Yamaguchi 2002, Chaudhuri and Chakraborty 2003, Moller *et al.* 2009) and there are several simulation methods that offer numerical solution of first-excursion problems with larger state-space dimensions (Au and Beck 2001a, b, Katafygiotis and Cheung 2006, Katafygiotis *et al.* 2007, Jensen and Valdebenito 2007).

There are usually two criteria for reliability evaluations of structures subjected to random earthquakes. One is the first excursion law and the other is the damage accumulation law. A method for dynamic reliability estimation based on damage accumulation of multi-grid composite walls is proposed in this paper. In order to research on the seismic performance of multi-grid composite wall structures, 13 multi-grid composite walls were tested. The equations including stiffness, shear forces when the filling blocks crack and when multi-grid composite walls yield, ultimate displacement, and damage index are obtained through the test results. Employing these equations in reliability estimations, procedures of dynamic reliability calculations of multi-grid composite walls subjected to random earthquake excitations are proposed. Random earthquake process samples are generated firstly, and then parameters of power spectral density function are determined in accordance with Chinese code for seismic design of buildings. The equivalent linearization equation of the system is presented as a state equation and then solved by the direct integration method, combined with Simpson numerical integration method and precise time-integration method. Finally, dynamic reliability estimation is presented based on damage accumulation. Define small earthquakes as earthquakes with 63% exceedence probability in a period of 50 years, and large earthquakes as earthquakes with 2-3% exceedence probability in a period of 50 years. The dynamic reliability

estimates, when the filling blocks crack under small earthquakes and when composite walls reach limit state under large earthquakes, are obtained using the proposed method by taking damage indexes as thresholds. The results from the proposed method which show good agreement with those from Monte-Carlo simulations demonstrate the proposed method is effective.

2. Tests of Multi-grid composite walls

13 multi-grid composite wall specimens that consist of one full scale specimen SW1 and twelve 1:2 scale specimens from SW3 to SW14 shown in Table 1 were tested (Jia *et al.* 2005). Horizontal loads acting on SW8, SW11 and SW14 were monotonic, on SW1, SW3, SW4, SW5, SW6, SW7, SW10, SW12 and SW13 were low-cycled. And load acting on SW9 was only vertical and monotonic. Fig. 2 illustrates the test set-up along with the mechanical model of specimen SW6, and Fig. 3 illustrates the diagrammatic sketch of specimen SW6. The vertical loads acting on the specimens were all 110 kN except SW7 with 65 kN and SW1 with 440 kN. Except that SW5 consisted of 3 grid columns, SW12 consisted of 5 grid columns and there was a window opening in SW11, the other tested walls all consisted of 4 grid columns and 4 grid beams. The diameter of longitudinal steel bars in grid columns of SW13 was different from that of other composite walls. For all the specimens the composite panel which was made up of filling blocks and RC grids connected with the bottom anchoring beam through mortar, and for SW14 the longitudinal steel bars of grid columns were fixed in the bottom anchoring beam additionally.

Tests on sample multi-grid composite walls have led to evaluate the following values:

(a) The elastic stiffness of multi-grid composite walls employing equivalent elastic plate model of composite material can be expressed as (Yu and Yao 2008)

Table 1 Tested multi-grid composite walls

	Dimension (m) (width×height×thickness)	Dimension of rectangular cross section (mm) (height×width) and longitudinal plain steel bars							
		Edge beam		Edge column		Grid beam		Grid column	
SW1	2.8×2.75×0.2	100×200	4Φ10	200×200	4Φ12	80×200	4Φ6	200×100	4Φ6
SW3	2.7×1.375×0.1	50×100	4Φ6	100×100	4Φ6	40×100	4Φ4	100×50	4Φ4
SW4	2.7×1.375×0.1	50×100	4Φ6	100×100	4Φ6	40×100	4Φ4	100×50	4Φ4
SW5	1.4×1.375×0.1	50×100	4Φ6	100×100	4Φ6	40×100	4Φ4	100×67	4Φ6
SW6	1.4×1.375×0.1	50×100	4Φ6	100×100	4Φ6	40×100	4Φ4	100×50	4Φ4
SW7	1.4×1.375×0.1	50×100	4Φ6	100×100	4Φ6	40×100	4Φ4	100×50	4Φ4
SW8	1.4×1.375×0.1	50×100	4Φ6	100×100	4Φ6	40×100	4Φ4	100×50	4Φ4
SW9	1.4×1.375×0.1	50×100	4Φ6	100×100	4Φ6	40×100	4Φ4	100×50	4Φ4
SW10	1.4×1.375×0.1	50×100	4Φ6	100×100	4Φ6	40×100	4Φ4	100×50	4Φ4
SW11	1.4×1.375×0.1	50×100	4Φ6	100×100	4Φ6	40×100	4Φ4	100×50	4Φ4
SW12	1.4×1.375×0.1	50×100	4Φ6	100×100	4Φ6	40×100	4Φ4	100×40	4Φ4
SW13	1.4×1.375×0.1	50×100	4Φ6	100×100	4Φ6	40×100	4Φ4	100×50	4Φ6
SW14	1.4×1.375×0.1	50×100	4Φ6	100×100	4Φ6	40×100	4Φ4	100×50	4Φ4

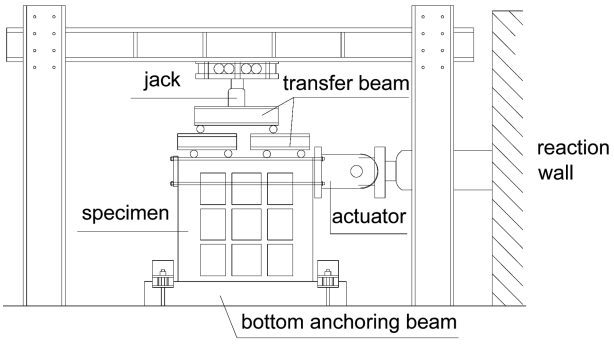

Fig. 2 Test set-up along with the mechanical model of specimen SW6

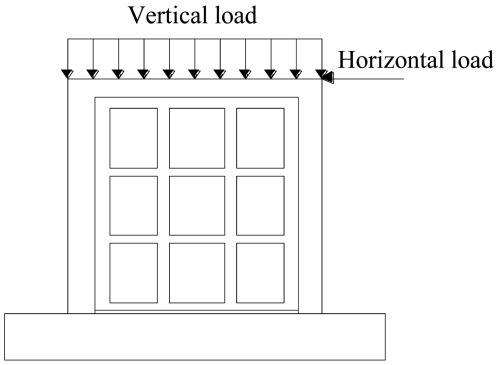

Fig. 3 Diagrammatic sketch of specimen SW6

$$k_s = \frac{\eta_c(2\eta_a + 0.4)}{\alpha_1\left(\frac{h^3}{12EI} + \frac{\gamma h}{GA}\right)} \tag{1}$$

in which $I = 1/12 t_h b^3$; $A = bt_h$; $E = \zeta V_c E_c + V_q E_q$; $1/G = V_c/G_c + V_q/G_q$; $\eta_a = N/(f_c A_c)$; $\eta_c = 1 + (n_b + n_c)/40$; h is the height of the composite wall; b is the width of the composite wall; t_h is the thickness of the composite wall; E_c, E_q, V_c, and V_q denote the elastic moduli of concrete and filling blocks, the volume fractions of concrete components and filling blocks in the composite wall respectively; G_c and G_q denote the shear moduli of concrete and filling blocks respectively; ζ is the modification factor of concrete and ζ = 07; γ is the non-uniform factor of shear stress and γ = 1.2 when the section is rectangular; η_a is the axial load ratio which has influence on the appearance and propagation of tiny and thin cracks influencing the elastic stiffness of composite walls and $0.3 \le \eta_a \le 0.6$; N, f_c and A_c denote the axial load acting on the composite wall, the compressive strength of concrete, and the concrete section area of grid columns and edge columns respectively; η_c is the constraint factor due to the influence of grid columns and grid beams on filling blocks; n_b is the number of grid beams and n_c is the number of grid columns; α_1 is the influence factor related to the connection form of the composite wall bottom: $\alpha_1 = 1$ when the connection is through mortar and $\alpha_1 = 0.9$ when the connection is reinforced.

Table 2 Stiffness of multi-grid composite walls

	k_s (kN/mm)	K_1 (kN/mm)	K_2 (kN/mm)	K_3 (kN/mm)	K_2/K_1 (kN/mm)	K_3/K_1 (kN/mm)
SW1	103.8	107.5	15.8	2.3	0.146	0.021
SW3	146.7	148.4	40.6	7.8	0.273	0.052
SW4	-	128	49.1	14.0	0.383	0.109
SW5	58.1	62.5	21.1	2.9	0.337	0.046
SW6	60.4	66	13.8	3.3	0.3	0.071
SW7	39.1	45	11.9	4.1	0.264	0.091
SW8	60.4	56.8	12.3	2.0	0.216	0.035
SW9	60.4	66.8	21.6	1.6	0.323	0.024
SW10	60.4	67.7	11.5	5.5	0.169	0.081
SW11	-	9.3	2.7	0.9	0.290	0.096
SW12	-	38	8.5	3.4	0.223	0.089
SW13	-	47.2	12.7	4.1	0.269	0.086
SW14	-	27.2	10.6	2.0	0.389	0.073

The elastic stiffness *ks* of Eq. (1), the pre-cracking stiffness K_1, the pre-yield stiffness K_2 and the post-yield stiffness K_3 from the test results (Yu and Yao 2008) are shown in Table 2, and then equations of stiffness for multi-grid composite walls are obtained.

The pre-cracking stiffness of composite walls is

$$K_1 = k_s \tag{2}$$

The pre-yield stiffness of composite walls is

$$K_2 = 0.22K_1 \tag{3}$$

The post-yield stiffness of composite walls is

$$K_3 = 0.05K_1 \tag{4}$$

(b) The shear force when the filling blocks crack can be written as (Yao *et al.* 2008)

$$F_k = \frac{\eta_c b t_h}{1.35} f_{tq} \sqrt{1 + \frac{\sigma_q}{f_{tq}}} \tag{5}$$

where $\sigma_q = \frac{b}{\left(\frac{E_c}{E_q} b_c + b_q\right)} \frac{N}{b t_h}$; f_{tq} and σ_q denote the tensile strength and the vertical compressive stress of filling blocks respectively; b_c denotes the section width of edge frame columns and grid columns; b_q denotes the section width of filling blocks.

The shear force when the multi-grid composite walls yield can be written as (Yao *et al.* 2008)

$$F_y = 0.85\left[\frac{1}{1 + 0.5\lambda}(0.4A_c f_t + 0.25A_q f_{tq} + 0.13N) + (n_b - 1) f_{yh} A_{sh} + 0.08(n_c + 1) f_{yv} A_{sv}\right] \tag{6}$$

Table 3 Yield shear forces of some multi-grid composite walls

	Test results (kN)	Calculated results (kN)
SW1	260	254
SW5	81	83
SW6	90	92
SW7	84	88
SW8	98.6	92
SW10	100	92
SW13	94	99
SW14	90	77

where f_t is the tensile strength of concrete; A_q is the section area of filling blocks; A_{sh} is the reinforcement area of one grid beam; A_{sv} is the reinforcement area of one grid column; f_{yh} is the design yield strength of reinforcement in grid beams; and f_{yv} is the design yield strength of reinforcement in grid columns (f_{yh} and f_{yv} are both smaller than or equal to 300 N/mm^2); λ is the height-width ratio of the composite wall and $1.0 \le \lambda \le 2.0$; for $N > 0.2 f_c A_c, N = 0.2 f_c A_c$.

The shear forces when the multi-grid composite walls yield calculated according to Eq. (6) by assuming the yield strengths of reinforcement equal to the design values show good agreement with the test results in Table 3. The yielding deformation was determined by the intersection of the horizontal line at maximum force with the straight line passing through the origin and the 75% maximum force point $F_{\max}$ on the envelope curve for the test results.

(c) The ultimate displacement of composite walls can be expressed as

$$X_u = \mu X_y \tag{7}$$

where μ denotes the ductility factor for composite walls; X_y denotes the yield displacement of composite walls and

$$X_y = \frac{F_k}{K_1} + \frac{F_y - F_k}{0.22 K_1} \tag{8}$$

Table 4 Ductility factors of some multi-grid composite walls

	Ultimate displacement x_u (mm)	Yield displacement x_y (mm)	Ductility factor μ
SW1	64.4	9.5	6.8
SW3	23.0	3.8	6.1
SW5	32.1	5.4	6.0
SW6	31.3	5.8	5.4
SW7	5.6	33.1	5.9
SW11	5.0	32.4	6.4
SW13	5.7	32.0	5.6
SW14	6.0	30.3	5.1

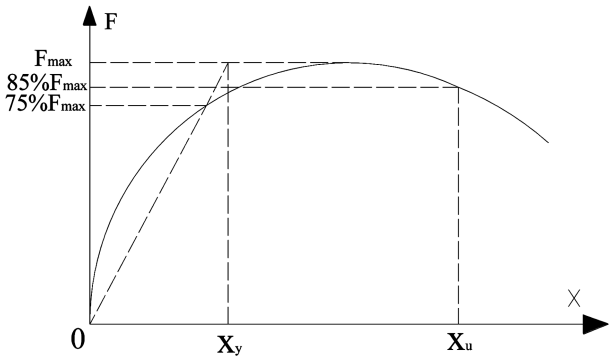

Fig. 4 Definition of yield and ultimate displacement

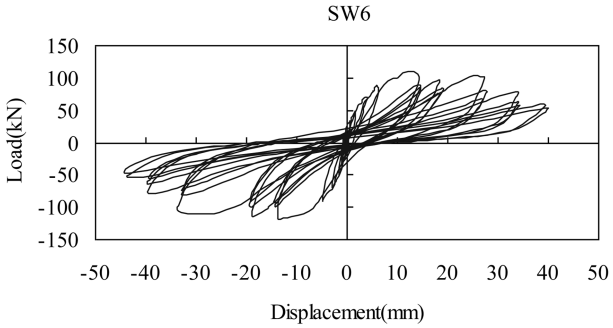

Fig. 5 Observed hysteresis loops diagram of specimen SW6

Table 5 Damage calibration factors of some multi-grid composite walls

	SW1	SW3	SW4	SW5	SW6	SW7	SW10	SW12	SW13
β	0.26332	0.27870	0.34015	0.24646	0.15393	0.20518	0.25458	0.33688	0.13254

The ductility factors of some multi-grid composite walls are shown in Table 4 according to the test results (Yuan *et al.* 2006), from which assume $\mu = 5.0$ for composite walls of shear failure. The displacement ductility factor of a specimen can be calculated as the ratio of tested ultimate displacement to yield displacement. The tested ultimate displacement is the lateral displacement when the lateral load fell to 85% of the maximum lateral load. Fig. 4 illustrates the definition of yield and ultimate displacement for the test results. The uncertainty of μ is neglected in the reliability calculations. The failure mode of SW6 is typical shear failure and the observed hysteresis loops diagram of SW6 is shown in Fig. 5.

(d) The damage calibration factors of some multi-grid composite walls are shown in Table 5 (Yuan *et al.* 2006). By employing the mean of the damage calibration factors in Table 5, the damage calibration factor of multi-grid composite walls adopts $\beta = 0.25$. The uncertainty of β is neglected in the reliability calculations.

The damage index D (Park and Ang 1985) of multi-grid composite walls is expressed as (Yuan *et al.* 2006)

Table 6 Damage indexes of multi-grid composite walls at filling blocks cracking

	x_u (mm)	F_y (kN)	X_m (mm)	β	$E_h(T)$ (kN·mm)	$F_y x_u$ (kN·mm)	Damage index
SW1	90	265	2	0.25	0	23850	0.0166667
SW3	34.2	220	1.2	0.25	0	7524	0.0263158
SW4	34.2	173	1.2	0.25	0	5916.6	0.0263158
SW5	44	77	0.8	0.25	0	3388	0.0136364
SW6	44	86	1.08	0.25	0	5784	0.0184091
SW7	44	80.5	0.89	0.25	0	3942	0.0151705
SW8	44	86	0.63	0.25	0	3784	0.0107386
SW9	44	110	0.61	0.25	0	4840	0.0103977
SW10	44	81	0.6	0.25	0	3564	0.0102273
SW11	44	33.5	3.7	0.25	0	1474	0.0630682
SW12	44	78	1.2	0.25	0	5432	0.0204545
SW13	44	94	0.8	0.25	0	6136	0.0136364
SW14	44	82	0.9	0.25	0	3608	0.0153409

Table 7 Damage indexes of multi-grid composite walls at composite walls reaching limit state

	x_u (mm)	F_y (kN)	X_m (mm)	β	$E_h(T)$ (kN·mm)	$F_y x_u$ (kN·mm)	Damage index
SW1	90	265	47.5	0.25	55358.35	23850	0.9761095
SW3	34.2	220	15	0.25	18456.28	7524	0.9421943
SW4	34.2	173	16.4	0.25	11890.3	5916.6	0.8620618
SW5	44	77	11	0.25	11157.2	3388	1.0107881
SW6	44	86	14.2	0.25	17870.63	5784	1.014462
SW7	44	80.5	17.9	0.25	11681.2	3942	1.0459305
SW8	44	86	42	0.25	4377.59	3784	1.0051262
SW9	44	110	42	0.25	7093.85	4840	1.082327
SW10	44	81	22	0.25	8781.85	3564	0.9910108
SW11	44	33.5	34	0.25	1650.53	1474	0.8594861
SW12	44	78	23	0.25	12656.22	5432	0.9745298
SW13	44	94	26	0.25	15209.76	6136	1.0628754
SW14	44	82	42	0.25	2776.01	3608	0.9082601

$$D = (1-\beta)\frac{X_m}{X_u} + \beta\frac{E_h(T)}{F_y X_u} \tag{9}$$

where X_m, X_u, F_y and $E_h(T)$ denote the maximum displacement under earthquake excitation, the ultimate displacement under monotonic loading, the calculated yield shear force and the accumulative hysteretic energy under earthquake excitation in the time interval [0, T] of the composite wall respectively.

The damage index values of multi-grid composite walls when the filling blocks crack are shown in Table 6, and they are shown in Table 7 when the composite walls reach limit state.

3. Dynamic reliability estimations of multi-grid composite walls

3.1 Simulation of the random earthquake process

Generate a discrete white noise signal $W(t_j) = \sqrt{2\pi S_0/\Delta t}\,\theta_j$, $j = 1, \ldots, T/\Delta t$ with the help of independent standard normal variables θ_j, where S_0 is the power spectral density, and T is the duration and $t_j = j\Delta t$.

Pass the signal through two discrete filters having the following continuous representation (Clough and Penzien 1993)

$$\ddot{a}(t) + 2\zeta_g\omega_g\dot{a}(t) + \omega_g^2 a(t) = W(t) \tag{10}$$

$$\ddot{x}_g(t) + 2\zeta_f\omega_f\dot{x}_g(t) + \omega_f^2 x_g(t) = 2\zeta_g\omega_g\dot{a}(t) + \omega_g^2 a(t) \tag{11}$$

The initial conditions for each of the above two equations are assumed to be zero. $\ddot{x}_g(t)$ is the simulated stationary earthquake ground acceleration.

3.2 Power spectral density function of the random earthquake process

The power spectral density function of the process $\ddot{x}_g(t)$ is introduced as (Clough and Penzien 1993)

$$S_{\ddot{x}_g}(\omega) = \frac{\omega_g^4 + 4\zeta_g^2\omega_g^2\omega^2}{(\omega_g^2 - \omega^2)^2 + 4\zeta_g^2\omega_g^2\omega^2} \cdot \frac{\omega^4}{(\omega_f^2 - \omega^2)^2 + 4\zeta_f^2\omega_f^2\omega^2} S_0 \tag{12}$$

where ζ_g and ω_g denote damping ratio of soil and characteristic frequency of soil respectively; ζ_f and ω_f are parameters for a high-pass filter to attenuate low frequency components, generally $\zeta_f = \zeta_g$ and $\omega_f = 0.1\omega_g$. Research on the above parameters was made according to Chinese code for seismic design of buildings (Xue *et al.* 2003).

Table 8 shows parameter values for different soil types and seismic design groups. The earthquake duration T, defined as the time when the amplitude of earthquake exceeds 50% of maximum amplitude, is shown in Table 9 for different soil types.

Table 8 Parameter values for different soil types and seismic design groups

Soil type		I	II	III	IV
ω_g (rad/s)	The first group	25.13	17.95	13.96	9.67
	The second group	20.94	15.71	11.42	8.38
	The third group	17.95	13.96	9.67	6.98
ζ_g		0.64	0.72	0.80	0.90

Table 9 Earthquake duration for different soil types

Soil type	I	II	III	IV
Duration(s)	6.69	8.41	10.92	15.49

Table 10 M, L and f for different soil types and design seismic groups

Soil type		I	II	III	IV
M		0.8847	0.8798	0.8694	0.8498
L (s^{-1})	The first group	122.72	94.59	76.12	56.31
	The second group	110.40	84.71	64.22	49.73
	The third group	97.03	76.61	55.53	42.29
f	The first group	3.122	3.160	3.224	3.301
	The second group	3.092	3.140	3.195	3.281
	The third group	3.066	3.122	3.170	3.255

Table 11 $\bar{a}_m$ (cm/s^2) for different seismic intensities

	Seismic intensity 6	Seismic intensity 7	Seismic intensity 8	Seismic intensity 9
Under small earthquakes	18	35	70	140
Under large earthquakes	-	220	400	620

The power spectral density corresponding to white noise S_0 can be written as

$$S_0 = \frac{\bar{a}_m^2}{MLf^2} \tag{13}$$

where M, L and f for different soil types and seismic design groups are shown in Table 10 and a set of $\bar{a}_m$ (the mean of peak ground accelerations) for different seismic intensities are shown in Table 11.

3.3 Equivalent linearization of the hysteretic system

The equation of motion for the system can be written in the form

$$m\ddot{X} + g(X, \dot{X}) = -m\ddot{x}_g(t) \tag{14}$$

where m is the mass, and $\ddot{x}_g(t)$ is a sample of random earthquake processes from Eq. (11).

Engineering structures often exhibit hysteretic behavior under severe cyclic load associated with earthquakes. The Bouc-Wen model (Wen 1980) is a smooth endochronic model that is often used to describe hysteretic phenomena. The model has been successfully employed in reinforced concrete and steel structures. The smooth hysteretic model has been well received in nonlinear stochastic dynamics not only because of its versatility through appropriate choices of parameters in the model but also for the possibility of calculating the linearization matrices in explicit form (Hurtado and Barbat 2000).

In terms of Bouc-Wen model

$$g(X, \dot{X}) = c\dot{X} + \alpha kX + (1-\alpha)kZ \tag{15}$$

where c is the damping of the system, the hysteretic part Z depends on nonhysteretic part X and $\dot{X}$ by means of an incremental relation. A smooth, hysteretic dependence is provided by the relation

$$\dot{Z} = H\dot{X} - \psi|\dot{X}||Z|^{i-1}Z - \delta\dot{X}|Z|^i \tag{16}$$

where $H=1, i=2, \psi=-3\delta$, and $\delta=-1/2[(1-\alpha)k/F_y]^2$ for reinforced concrete structures, and here assume they are applicable to multi-grid composite walls; α is the ratio of post-yield to pre-yield stiffness which can be determined by Eq. (3) and Eq. (4); k is the pre-yield stiffness which can be determined by Eq. (3); F_y is the shear force of yield which can be determined by Eq. (6).

Eq. (16) can be replaced by the linearized form

$$\dot{Z} = C_e\dot{X} + K_e Z \tag{17}$$

$$C_e = 1-\frac{2}{\pi}\psi\sigma_Z^2\times\left[\frac{\pi}{2}-\arctan\left[\frac{\sqrt{1-\rho_{\dot{X}Z}^2}}{\rho_{\dot{X}Z}}\right]+\rho_{\dot{X}Z}\sqrt{1-\rho_{\dot{X}Z}^2}\right]-\delta\sigma_Z^2 \tag{18}$$

$$K_e = -\psi\frac{4}{\pi}\sigma_{\dot{X}}\sigma_Z\times\left\{(1-\rho_{\dot{X}Z}^2)^{3/2}+\rho_{\dot{X}Z}\times\left[\frac{\pi}{2}-\arctan\frac{\sqrt{1-\rho_{\dot{X}Z}^2}}{\rho_{\dot{X}Z}}+\rho_{\dot{X}Z}\sqrt{1-\rho_{\dot{X}Z}^2}\right]\right\}-2\delta E[\dot{X}Z] \tag{19}$$

in which $\rho_{\dot{X}Z}=E[\dot{X}Z]/\sigma_{\dot{X}}\sigma_Z$.

By introducing the state vector $\{Y\}=\{X,\dot{X},Z\}^T$, the equation of motion can be written as

$$\{\dot{Y}(t)\} = [A]\{Y(t)\}+\{B\}\ddot{x}_g(t) \tag{20}$$

where $[A]=\begin{bmatrix}0 & 1 & 0\\ -\alpha k/m & -c/m & -(1-\alpha)k/m\\ 0 & C_e & K_e\end{bmatrix}$, $\{B\}=\{0\ \ -1\ \ 0\}^T$.

3.4 Solution of the state equation

The exact solution of Eq. (20) using direct integration method (Zhang and Cao 2000) can be expressed as

$$\{Y(t)\} = \exp([A]\cdot t)\{Y(0)\}+\int_0^t\exp([A]\cdot(t-\tau))\{B\}\ddot{x}_g(\tau)d\tau \tag{21}$$

Evaluating $\{Y(t)\}$ at discrete values of t_j, then

$$\{Y(t_j)\} = \exp([A]\cdot\Delta t)\{Y(t_{j-1})\}+\int_{t_{j-1}}^{t_j}\exp([A]\cdot(t_j-\eta))\{B\}\ddot{x}_g(\eta)d\eta \tag{22}$$

Assuming $[T_e]=\exp([A]\cdot\Delta t)$ and employing Simpson numerical integration method, the integration of the second term of Eq. (22) can be expressed as

$$\int_{t_{j-1}}^{t_j}\exp([A](t_j-\eta))\{B\}\ddot{x}_g(\eta)d\eta$$

$$=\frac{\Delta t}{6}\left([T_e]\{B\}\ddot{x}_g(t_{j-1})+4[T_1]\{B\}\ddot{x}_g\left(t_{j-1}+\frac{1}{2}\Delta t\right)+\{B\}\ddot{x}_g(t_j)\right)+o(\Delta t^5) \tag{23}$$

where $[T_1]=\exp\left([A]\cdot\frac{1}{2}\Delta t\right)$.

Then Eq. (22) can be written as

$$\{Y(t_j)\} = [T_e]\{Y(t_{j-1})\} + \frac{\Delta t}{6}\left([T_e]\{B\}\ddot{x}_g(t_{j-1}) + 4[T_1]\{B\}\ddot{x}_g\left(t_{j-1}+\frac{1}{2}\Delta t\right) + \{B\}\ddot{x}_g(t_j)\right) \tag{24}$$

The solution of exponential matrix is accurate enough, so the error in Eq. (24) which comes from the error of Simpson integration is small and can be generally expressed as $\varepsilon = o(\Delta t^5)$.

$[T_e]$ and $[T_1]$ in Eq. (24) can be solved by precise time-integration method (Zhang and Zhong 2000) and the detail procedures are as follows: the additive rule of exponential matrix is

$$[T_e] = \exp([A]\cdot\Delta t) = (\exp([A]\cdot\Delta t/n))^n \tag{25}$$

where $n = 2^J$, generally for $J = 20$, and $n = 1048576$.

For a time interval $\Delta t/n$ which is much smaller than Δt

$$\exp([A]\cdot\Delta t/n) \approx [I] + [A]\cdot\Delta t/n + \frac{1}{2}([A]\cdot\Delta t/n)^2 = [I] + [T_a] \tag{26}$$

where $[I]$ is a unit matrix that is of the same order as $[A]$, and $[T_a] = ([A]\cdot\Delta t/n)\left([I]+\frac{1}{2}[A]\cdot\Delta t/n\right)$.

$[T_a]$ rather than $[I]+[T_a]$ is used to avoid the round off error and truncation error dominating the calculations because $[T_a]$ is relatively small, and Eq. (25) is rewritten as

$$[T_e] = ([I]+[T_a])^{2^J} = ([I]+[T_a])^{2^{J-1}} \times ([I]+[T_a])^{2^{J-1}} \tag{27}$$

Instead of operating unit matrix $[I]$ in the addition and multiplication, calculate Eq. (28) for J times

$$[T_a] = 2[T_a] + [T_a]\times[T_a] \tag{28}$$

in which $[T_a]$ on the right hand side adopts the value calculated in the previous cycle. Then the final result $[T_e] = [I]+[T_a]$.

3.5 The mean and the variance of damage index

According to the expression of damage index of multi-grid composite walls, by assuming that X_m and $E_h(T)$ are correlated fully the mean and the variance of damage index can be written as

$$E(D) = (1-\beta)\frac{E(X_m)}{X_u} + \beta\frac{E[E_h(T)]}{F_y X_u} \tag{29}$$

$$\sigma_D^2 = (1-\beta)^2\frac{\sigma_{X_m}^2}{X_u^2} + \frac{2\beta(1-\beta)}{F_y X_u^2}\sigma_{X_m}\sigma_{E_h(T)} + \frac{\beta^2}{F_y^2 X_u^2}\sigma_{E_h(T)}^2 \tag{30}$$

F_y and X_u can be determined by Eqs. (6) and (7), and $\beta = 0.25$.

For the stationary Gaussian process $X(t)$, the mean and the variance of maximum displacement and accumulative hysteretic energy can be written as

$$E(X_m) = \gamma_m \sigma_X \tag{31}$$

$$E[E_h(T)] = (1-\alpha)kE[Z(t)\dot{X}(t)]T \tag{32}$$

$$\sigma^2_{X_m} = \Delta^2_m \sigma^2_X \tag{33}$$

$$\sigma^2_{E_h(T)} = E[E^2_h(T)] - \{E[E_h(T)]\}^2 \tag{34}$$

where $\gamma_m = \sqrt{2\ln(\nu_{0X}T)} + \dfrac{0.5772}{\sqrt{2\ln(\nu_{0X}T)}}$; $\nu_{0X} = \dfrac{1}{\pi}\dfrac{\sigma_{\dot{X}}}{\sigma_X}$, in which σ_X and $\sigma_{\dot{X}}$ are the standard deviations of $X(t)$ and $\dot{X}(t)$ respectively; $\Delta_m = \dfrac{\pi}{\sqrt{12\ln(\nu_{0X}T)}}$ (Song and Grigoriu 1993); $E[E^2_h(T)] = (1-\alpha^2)k^2T^2 \times \{E[Z^2(t)]E[X^2(t)] + 2[E(Z(t)\dot{X}(t))]^2\}$.

Eq. (31) to Eq. (34) can be derived from sections 3.3 and 3.4.

3.6 Dynamic reliability estimation based on damage accumulation

The probability density function of random accumulative damage index D that follows logarithmic normal distribution is

$$p_D(d) = \frac{1}{\sqrt{2\pi}\sigma_\xi d}\exp\left\{-\frac{[\ln d - E(\xi)]^2}{2\sigma^2_\xi}\right\} \tag{35}$$

where $\xi = \ln D$; $E(\xi) = \ln E(D) - \dfrac{1}{2}\ln(1+V^2_D)$; $\sigma^2_\xi = \ln(1+V^2_D)$; $V_D = \sigma_D/E(D)$.

Then dynamic reliability estimate $\hat{p}_s$ based on damage accumulation is

$$\hat{p}_s(D < D_0) = \int_0^{D_0} p_D(s)ds \tag{36}$$

where D_0 denotes the threshold of damage index.

4. Example

Consider that the multi-grid composite wall specimen SW6 shown in Fig. 6 is subjected to random earthquake excitations, and the vertical load acted on SW6 is 110 kN. The concrete class is C25, the grade of longitudinal steel bars is HPB235, the tensile strength of the filling blocks is 0.3 MPa, and the elastic modulus of the filling blocks is 2×10^3 MPa for SW6. The proposed method in this paper is used to calculate dynamic reliability estimates of SW6. By assuming seismic intensity is 8, the design seismic group is the first group, and the soil type is III according to Chinese code for seismic design of buildings, and then $T = 10.92$s, $\Delta t = 0.01$ s, for small earthquakes $S_0 = 7.1234 \times 10^{-4}\,\mathrm{m^2/s^3}$ and for large earthquakes S_0=$232.6010 \times 10^{-4}\,\mathrm{m^2/s^3}$. The random variables describing random earthquake excitations are the standard normal random variables in Eq. (10). A sample of stationary random process under small earthquakes is shown in Fig. 7 and a sample under

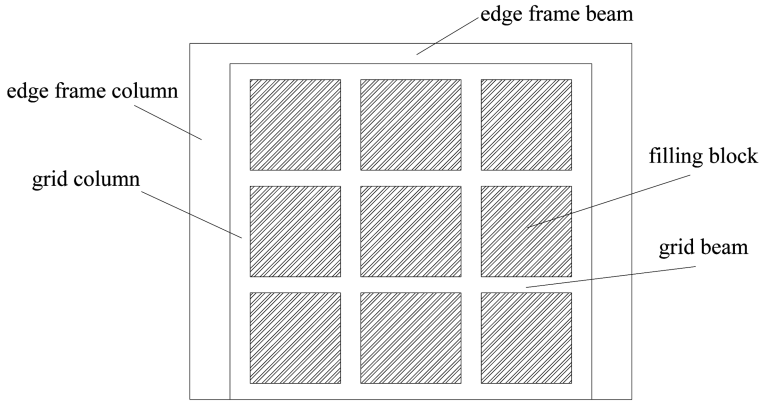

Fig. 6 Multi-grid composite wall specimen SW6

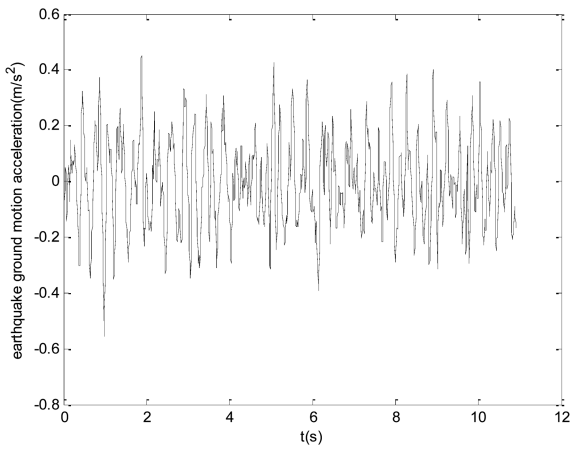

Fig. 7 A sample of stationary random process under small earthquakes

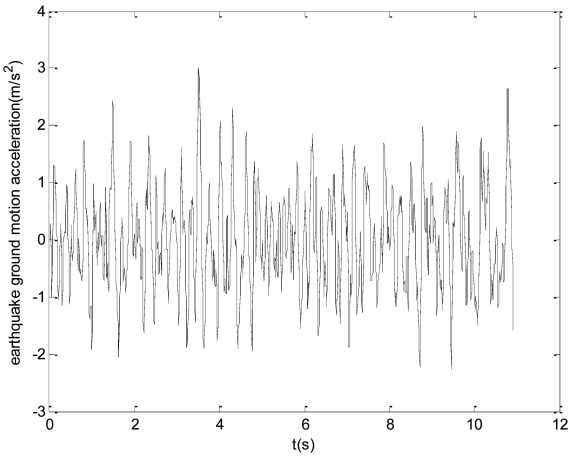

Fig. 8 A sample of stationary random process under large earthquakes

large earthquakes is shown in Fig. 8.

According to the results obtained from the tests in Table 6 and Table 7, assume that the damage index threshold is $D_0 = 0.02$ when filling blocks crack under small earthquakes and $D_0 = 0.95$ when the composite wall reaches limit state under large earthquakes. The uncertainty of the damage index thresholds is neglected in the reliability calculations.

The numerical simulation procedures of dynamic reliability estimations are as follows:

(a) Generate random earthquake process samples.

(b) Assume initial equivalent damping coefficient and equivalent stiffness coefficient for iteration. Solve structural responses and their statistical values using the equivalent linearized state equation; through direct integration method combined with Simpson integration method and precise time-integration method the state equation can be solved; according to the response statistical values update the equivalent damping coefficient and equivalent stiffness coefficient. The iteration needs to be repeated until the equivalent damping coefficient and equivalent stiffness coefficient in two

consecutive iterations is sufficiently close.

(c) Using the response statistical values in the final iteration, the dynamic reliability estimates are obtained when the filling blocks crack under small earthquakes and when the composite wall reaches limit state under large earthquakes.

The key parameter describing the computational effort is the number of sample random processes generated. The reliability estimates $\hat{p}_s$ for sample size N_p ranging from 5 to 50, when the filling blocks crack under small earthquakes with damage index threshold 0.02 and when the composite wall reaches limit state under large earthquakes with damage index threshold 0.95, are shown in Fig. 9. For each sample size, the statistical variability of the reliability estimate is assessed using 50 simulation runs, and the reliability estimate of each sample size in Fig. 7 adopts the mean of results of 50 simulation runs.

Monte-Carlo method is a general method for dynamic reliability estimations and can be used for the accuracy checking of the proposed method. The coefficient of variation (COV) of failure probability p_f obtained by Monte-Carlo method is given by $\mathrm{COV} \approx \sqrt{1/(p_f N_s)}$, where N_s is the number of simulation random process samples of Monte-Carlo method. The ratio of total number of failures N_f to the number of simulated samples N_s is used as an estimate of failure probability p_f, and $p_f \approx \hat{p}_s = N_f/N_s$, and then the probability of reliability $p_s = 1 - p_f$ for Monte-Carlo method.

The results of dynamic reliability obtained by the proposed method using 20 samples and by Monte-Carlo method are shown in Table 12.

In Table 12, the reliability estimate obtained from the proposed method when the filling blocks crack under small earthquakes with $D_0 = 0.02$ shows good agreement with result obtained from Monte-Carlo method, and it is the same when the composite wall reaches limit state under large earthquakes with $D_0 = 0.95$. The reliability when $D_0 = 0.95$ decreases compared with that when $D_0 = 0.02$. And when $D_0 = 0.95$ the sample size needed for Monte-Carlo method to reach the same accuracy level (or COV) also decease compared with that when $D_0 = 0.02$. Only with a small number of samples, the COV obtained by the proposed method is already within high level of accuracy and smaller than that of Monte-Carlo method. The number of samples required by the proposed method is significantly smaller than that of Monte-Carlo method. In addition for example, the reliability estimate 0.9881 obtained from the proposed method under small earthquakes means that there is a 0.0119 failure probability of the damage index exceeding the threshold 0.02.

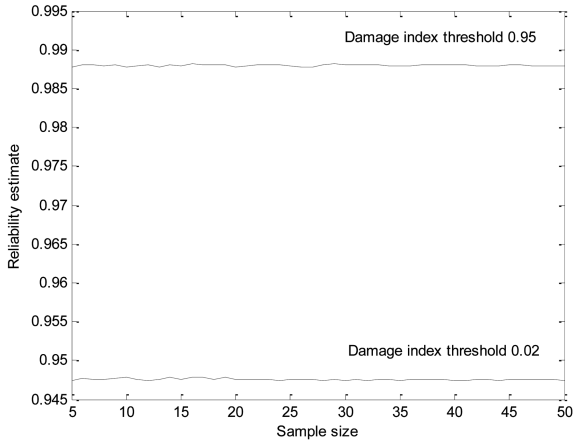

Fig. 9 Reliability estimates of SW6 for different threshold levels and number of samples

Table 12 Results of dynamic reliability of multi-grid composite wall specimen SW6 for different threshold levels

		Reliability result	COV	Sample size
$D_0 = 0.02$	Proposed method	0.9881	1.10%	20
	Monte-Carlo method	0.9882	13.02%	5000
$D_0 = 0.95$	Proposed method	0.9477	1.90%	20
	Monte-Carlo method	0.9475	9.76%	2000

5. Conclusions

In this study, a method for dynamic reliability calculations based on damage accumulation of multi-grid composite walls is proposed. Through calculations of the multi-grid composite wall specimen SW6 subjected to random earthquake excitations, the dynamic reliability estimates when the filling blocks crack under small earthquakes and when the composite wall reaches limit state under large earthquakes are obtained using the proposed method. Comparison with Monte-Carlo simulations indicates that results of the proposed method are in good agreement with them. The small number of simulation samples needed and the small COV indicate the proposed method is efficient. The use of equations determined through the tests shows an effective way to estimate dynamic reliabilities. The method proposed for dynamic reliability calculations of multi-grid composite walls, is also applicable to other structures with appropriate modifications.

Acknowledgements

This paper is based upon work partly supported by the Nation Natural Science Foundation of China (NO.50878021), the key project in the National Science and Technology Pillar Program during the eleventh Five-year Plan Period of China (NO.2006BAJ04A02-5), and Science and Technology Foundation for excellent Ph.D candidates in Beijing Jiaotong University (NO.141053522) of China.

References

Augusti, G. and Ciampoli, M. (2008), "Performance-based design in risk assessment and reduction", *Probabilist Eng. Mech.*, **23**(4), 496-508.

Au, S.K. and Beck, J.L. (2001), "Failure excursion probabilities for linear systems by efficient importance sampling", *Probabilist Eng. Mech.*, **16**(3), 193-207.

Au, S.K. and Beck, J.L. (2001), "Estimation of small failure probabilities in high dimensions by subset simulation", *Probabilist Eng. Mech.*, **16**(4), 263-277.

Chaudhuri, A. and Chakraborty, S. (2003), "Reliability evaluations of 3-D frame subjected to non-stationary earthquake", *J. Sound Vib.*, **259**(4), 797-808.

Chau, K.W. (2007), "Reliability and performance-based design by artificial neural network", *Adv. Eng. Softw.*, **38**(3), 145-149.

Chau, K.W. and Albermani, F. (2003), "Knowledge-based system on optimum design of liquid retaining

structures with genetic algorithms", *J. Struct. Eng.-ASCE*, **129**(10), 1312-1321.
Cheng, C.T., Chau, K.W. and Li, X.Y. (2007), "Hydrologic uncertainty for Bayesian probabilistic forecasting model based on BP ANN", *Proceedings of the third IEEE International Conference on Natural Computation*, Haikou, China, August.
Clough, R.W. and Penzien, J. (1993), *Dynamics of Structures*, 2nd edition, McGraw Hill, Inc., New York.
Dymiotis, C., Kappos, A.J. and Chryssanthopoulos, M.K. (1999), "Seismic reliability of RC frames with uncertain drift and member capacity", *J. Eng. Mech.-ASCE*, **125**(9), 1038-1047.
Dymiotis, C., Kappos, A.J. and Chryssanthopoulos, M.K. (2001), "Seismic reliability of masonry-filled RC frames", *J. Eng. Mech.-ASCE*, **127**(3), 296-305.
Hurtado, J.E. and Barbat, A.H. (2000), "Equivalent linearization of the Bouc-Wen hysteretic model", *Eng. Struct.*, **22**(2), 1121-1132.
Jensen, H.A. and Valdebenito, M.A. (2007), "Reliability analysis of linear dynamical systems using approximate representations of performance functions", *Struct. Saf.*, **29**(3), 222-237.
Jia, Y.J., Yuan, Q. and Yao, Q.F. (2005), "Study on seismic behavior of multi-ribbed slab structures", *Proceedings of the International Symposium on Innovation and Sustainability of Structures in Civil Engineering-Including Seismic Engineering*, Nanjing, China, November.
Katafygiotis, L.S. and Cheung, S.H. (2006), "Domain decomposition method for calculating the failure probability of linear dynamic systems subjected to Gaussian stochastic loads", *J. Eng. Mech.-ASCE*, **132**(5), 475-486.
Katafygiotis, L.S., Moan, T. and Cheung, S.H. (2007), "Auxiliary domain method for solving multi-objective dynamic reliability problems for nonlinear structures", *Struct. Eng. Mech.*, **25**(3), 402-423.
McMillan, H.K. and Brasington, J. (2008), "End-to-end flood risk assessment: A coupled model cascade with uncertainty estimation", *Water Resour. Res.*, **44**(3), W03419.
Moller, O., Foschi, R.O. and Rubinstein, M. (2009), "Seismic structural reliability using different nonlinear dynamic response surface approximations", *Struct. Saf.*, **31**(5), 432-442.
Park, Y.J. and Ang, A.H. (1985), "Mechanistic seismic damage model for reinforced concrete", *J. Struct. Eng.-ASCE*, **111**(4), 722-739.
Song, T.T. and Grigoriu, M. (1993), *Random Vibration of Mechanical and Structural Systems*, Prentice-Hall, Inc., Englewood Cliffs, New Jersey.
Takada, T. and Yamaguchi, K. (2002), "Two-step seismic limit state design procedure based on non-linear LRFD and dynamic response analyses", *Struct. Saf.*, **24**(2), 397-415.
Wen, Y.K. (1976), "Method for random vibration of hysteretic systems", *J. Eng. Mech. Div.-ASCE*, **102**(2), 249-263.
Xue, Q. and Chen, C.C. (2003), "Performance-based seismic design of structures: a direct displacement-based approach", *Eng. Struct.*, **25**(14), 1803-1813.
Xue, S.D., Wang, X.S. and Cao, Z. (2003), "Parameters study on seismic random model based on the new seismic code", *China Civil Eng. J.*, **36**(5), 5-10. (in Chinese)
Yao, Q.F., Hou, L.N. and Huang, W. (2008), "Shear capacity of multi-ribbed composite wall", *Proceedings of the tenth International Symposium on Structural Engineering for Young Experts*, Changsha, China, October.
Yuan, Q., Yao, Q.F. and Jia, Y.J. (2006), "Study on hysteretic model and damage model of multi-ribbed composite wall", *Proceedings of the International Symposium on Environmental Ecology and Technology of Concrete*, Urumqi, China, June.
Yu, X.F. and Yao, Q.F. (2008), "Stiffness research of multi-ribbed composite slab based on composite material model", *Proceedings of the Tenth International Symposium on Structural Engineering for Young Experts*, Changsha, China, October.
Zhang, H.W. and Zhong, W.X. (2000), "Discussion about numerical computation of the matrix exponential", *J. Dalian Univ. Technol.*, **40**(5), 522-525. (in Chinese)
Zhang, J.S. and Foschi, R.O. (2004), "Performance-based design and seismic reliability analysis using designed experiments and neural networks", *Probabilist Eng. Mech.*, **19**(3), 259-267.
Zhang, S.W. and Cao, K.B. (2000), "Direct integration of state equation method for dynamic response of structure", *Chinese J. Comput. Mech.*, **17**(1), 94-97. (in Chinese)